Photophysics and Solar Cell Application of a Benzodithiophene Conjugated Polymer Containing Cyclometalated Platinum Units

Ethan D. Holt,[†] Jiliang Wang,[†] Russell W. Winkel,[†] Younus Mohammed,[‡] and Kirk S. Schanze*[‡]

[†]Department of Chemistry, University of Florida, P.O. Box 117200, Gainesville, FL 32611-7200, United States

[‡]Department of Chemistry, University of Texas at San Antonio, One UTSA Circle, San Antonio, TX, 78249, United States

ABSTRACT

Cyclometalated platinum(II) chromophores were combined with benzodithiophene (BDT) units to form a conjugated molecule and polymer in order to ascertain their photophysical and electrochemical properties, as well as their potential for use in bulk heterojunction organic solar cells. Weak fluorescence and room temperature phosphorescence were observed for both the small molecule model complex and polymer, leading to the assumption that the presence of platinum metal centers serves to enhance intersystem crossing (ISC). Nanosecond and picosecond transient absorption spectroscopy were employed to study the excited state dynamics which revealed ISC rates of the polymers ($3x10^{12}$ s^{-1}) is faster than that of the model ($2.5x10^{11}$ s^{-1}). These fast ISC rates ensure a high population of triplet excited states, which was confirmed by singlet oxygen sensitization measurements. A laser power dependence of the triplet yield was observed to be more pronounced for the polymer, likely due to triplet-triplet annihilation within single polymer chains. Unfortunately, energy level estimations from electrochemistry and emission spectra placed the triplet state at or below energy of the charge transfer state to $PCB_{71}M$ acceptor. Organic solar cells were constructed using the model or polymer as donor in conjunction with $PC_{71}BM$ as acceptor. The polymer donor, provided the higher photocurrent efficiency at just over 1% in a non-optimized device.

Table of Contents Graphic

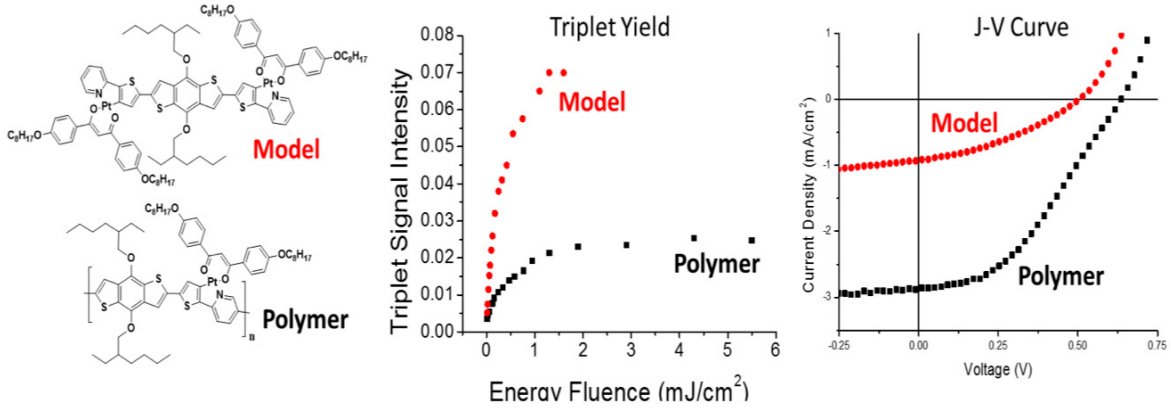

INTRODUCTION

With enough energy illuminating the earth's surface every hour to power the planet for an entire year,[1] the potential of solar energy to solve the world's energy problems is unchallenged. Even so, the high cost of silicon processing and low efficiencies of organic materials remain as significant roadblocks to the realization of that potential. Although silicon cells have plateaued at around 25% efficiency over the last 15 years,[2] organic photovoltaics have shown some of the most promising growth in the field, now reaching efficiencies approaching 18%.[3-7] Four key processes drive photocurrent generation in organic devices: (1) photon absorption by the active layer followed by exciton generation, (2) exciton diffusion, (3) charge transfer and exciton dissociation, and (4) charge collection.[4] The invention of the bulk heterojunction[8-9] along with properly tuned frontier orbital alignment have effected high efficiencies in the latter two processes. Photon absorption is largely improved by reducing the optical bandgap and thereby extending the spectral coverage of the donor molecule, where an ideal bandgap value of 1.5 eV (~ 825 nm) well balances the opposite dependence of the open-circuit voltage.[10-11] Exciton diffusion is strongly influenced by extent of conjugation and active layer morphology as the likelihood of recombination increases as exciton formation occurs further from the donor-acceptor interface.[12]

Because exciton diffusion length is directly proportional to excited state lifetime,[13-14] efforts to extend lifetimes of excited state chromophores may lead to improved photocurrent generation in devices. A potential advantage of organometallic π-conjugated small molecules and polymers is the incorporation of heavy metals which lead to high triplet populations through efficient singlet to triplet intersystem crossing (ISC).[15] Accessing high triplet populations may lead to increased exciton lifetimes as triplet decay is spin forbidden. In particular, the high spin-orbit coupling constant of platinum[16] has been shown to increase the rate of ISC and provide enhanced triplet

yield. Platinum poly-yne π-conjugated systems (e.g. [-PtL_2-CC-Ar-CC-]$_n$) have been well studied[15,17-22] and in at least one case, a decrease in conjugation was observed with platinum content due to improper Pt-C orbital overlap.[15] The cyclometalated architecture in which the platinum is attached via a C^N ligand has received increased attention recently.[23-26] In this motif, the metal center is coupled to the conjugated backbone via orthometallation within a coordination environment that is part of the π-conjugated network. These systems display enhanced conjugation compared to platinum poly-ynes. In the latter the platinum center is in the π-conjugated pathway of the polymer backbone, but the ancillary ligands (usually PR_3) distort the backbone planarity and can also disrupt inter-chain interactions due to unfavorable steric interactions.[25] The enhanced planarity of the cyclometalated motif may also lead to improved interchain interactions in the active layer of devices, which may serve to enhance charge transport in a film. The electron-rich platinum(II) center imparts efficient donor properties to these moieties and the cyclometalated structure has been successfully combined with acceptor units to form donor-acceptor (D-A) conjugated small molecules and polymers for use in solar cell applications.[23-24,26-27]

Benzo[1,2-b:4,5-b']dithiophene (BDT) is a versatile organic building block that has found wide use in organic electronics, including hundreds of research studies on organic solar cells.[28] The majority of solution processed organic solar cells with efficiencies over 10% incorporate BDT as a donor moiety, either in polymer or small molecule form.[29-32] The planar fused aromatic core results in efficient π–π stacking between adjacent molecules, leading to enhanced interchain hole mobility and large domain sizes.[33-36] Further, the BDT core is flexible to substitution and conjugation can be extended from the core in two planes, in-line with the fused thiophene rings or orthogonally from the 4,8 positions on the central benzene ring.[31,37-40]

Drawing from recent successes in the coupling of cyclometalated platinum(II) donor chromophores with acceptors showing strong spin-orbit coupling and excited state delocalization,[24-25] we pursued the synthesis, photophysical and organic solar cell characterization of the BDT-coupled cyclometalated Pt(II) materials shown in Chart I. (Note that the repeat unit of the polymer p-BDT-Pt is regiorandom.) Complete photophysical characterization of the materials was accomplished through ground-state absorption, steady-state emission, and transient absorption (TA) spectroscopy. Although analysis of charge transfer energetics suggests that photoinduced charge transfer to $PCB_{71}M$ (phenyl-C71-butyric acid methyl ester) should be inefficient, a modest power conversion efficiency of just over 1% was achieved in non-optimized devices utilizing p-BDT-Pt in the active layer. Excitation power dependent transient absorption studies further revealed a rapid decay process for triplet excited states in p-BDT-Pt, and the process is attributed to triplet-triplet annihilation (TTA). Through this unique molecular structure, interesting photophysical properties are observed including TTA, that may expand the scope of application for conjugated materials in organic electronics.

Chart 1

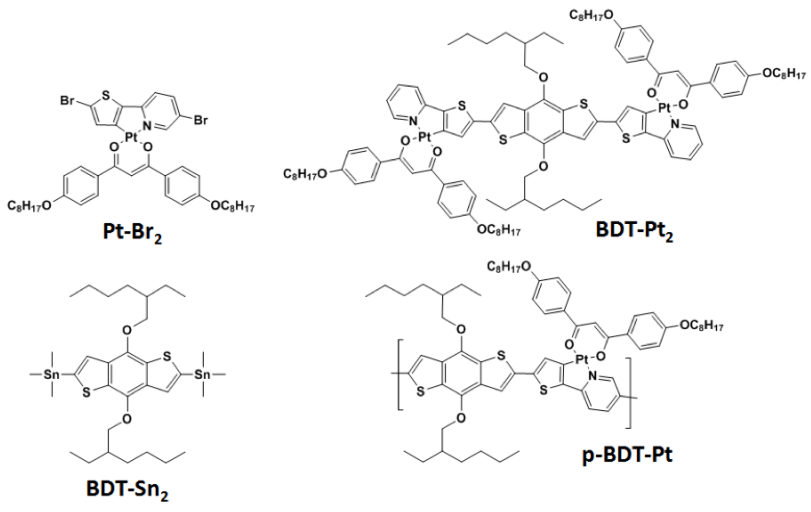

EXPERIMENTAL

Synthesis. Details of synthetic procedures and structural characterization are contained in the supporting information.

Instrumentation and Methods. NMR spectra were recorded using a Varian-Inova-500 FT-NMR (500 MHz for ^{1}H, 125 MHz for ^{13}C) or a Mercury-300 FT-NMR (300 MHz for ^{1}H). Mass spectra were obtained by the University of Florida Mass Spectrometry Facility. Polymer molecular weights were determined using a Shimadzu gel permeation chromatography setup with LC-6AD Liquid Chromatograph at a concentration of 1 mg/ml in THF with polystyrene standard.

All photophysical measurements were performed using dry, HPLC-grade THF in 1×1 cm^2 cuvettes. Steady-state absorption measurements were obtained using a Shimadzu UV-1800 dual beam spectrophotometer. Steady-state photoluminescence spectra were obtained using a Photon Technology International (PTI) spectrophotometer and collected by a PTI 814 photomultiplier tube detector at 90° relative to the excitation beam. Solution samples were taken in THF with an optical density of ~ 0.1 at the excitation wavelength. Phosphorescence emission measurements were conducted after degassing the solution with argon for at least 30 minutes. Phosphorescence quantum yield measurements were made following five freeze-pump-thaw cycles. Singlet oxygen sensitization measurements were performed with a PTI fluorimeter equipped with near-IR detector. The emission was passed through an 830 nm long-pass filter to block the second multiple of the excitation source. Compounds were dissolved in $CDCl_3$ after passing the solvent through a column of basic alumina to remove residual DCl. Solutions were then purged with O_2 for 10 minutes prior to measurement. Fluorescence lifetime measurements were acquired with a PicoQuant FluoTime 100 Compact Fluorescence Lifetime Spectrometer using time-correlated

single photon counting (TCSPC). Samples were excited using a PDL-800B picosecond pulsed diode laser (375 nm).

Electrochemical measurements (CV and DPV) were acquired using a CHI-660E electrochemical workstation with a 2 mm diameter platinum working electrode, Ag/Ag^+ reference electrode and platinum wire counter electrode. Samples dissolved in dry CH_2Cl_2 were tuned to a concentration of ~ 1 mM, mixed with 0.1 M tetra-*n*-butylammonium hexafluorophophate (NBu_4PF_6) and purged with argon for 20 minutes. Measurements on film samples (drop cast directly onto the working electrode from THF and allowed to air dry) were conducted in HPLC-grade acetonitrile with 0.1 M NBu_4PF_6 supporting electrolyte after 20 minutes of argon purging. Experiments were conducted under argon with a scan rate of 100 mV/s.

Nanosecond transient absorption samples were prepared in 1 cm^2 flow cells with continuous circulation in deoxygenated (45 min argon bubbling) THF at OD ~ 0.7. Measurements were conducted using an in-house apparatus pumped by a Continuum Surelight Nd:YAG laser (355 nm, 10 ns FWHM, 10 mJ/pulse). Samples were probed by a xenon flash lamp and detected by a gated intensified CCD array mounted on a 0.18 M spectrograph (Princeton PiMax/Acton Pro 180). The initial CCD picture was taken 50 ns after excitation and subsequent pictures at an interval appropriate to the specific lifetime. Triplet lifetimes for uniform decay profiles were calculated using SpecFit analysis software as the single exponential global fit of the TA decay data. Energy dependence experiments and polymer triplet lifetime measurements were conducted at a single wavelength on an in-house spectrometer using a Continuum Surelite II-10 Nd:YAG laser as pump source, xenon arc lamp as probe source, Triax 180 monochromator, and Thorlabs Si amplified photodetector (PDA8A).

Femtosecond/picosecond TA measurements were performed on an Ultrafast Systems Helios Fire transient absorption spectrometer. The output beam (800 nm) of a Coherent Astrella Ti:saphire pulsed laser (120 fs, 1 kHz) was split into pump and probe beams. The pump was passed through a Coherent OPerA Solo optical parametric amplifier to tune the excitation wavelength (290-2600 nm) prior to entering the spectrometer. Inside the spectrometer, the pump was passed through a mechanical chopper, depolarizer, and neutral density filter to tune the pump power to 0.1 mW (100 nJ/pulse). The probe beam entered the spectrometer and passed through a computer-controlled 8 ns delay stage and wavelength specific crystals to adjust the spectral region of the probe beam (sapphire for visible, 420-780 nm; and an Ultrafast Systems proprietary crystal for NIR, 820-1500 nm). Samples in deoxygenated THF were tuned to an optical density of ~ 0.2 and continuously stirred in a cuvette with 2 mm pathlength at the location of pump-probe overlap, where the laser spot size was ~ 435 μm. Signal from the probe beam was detected using a fiber-coupled alignment free spectrometer at either a visible (1024 pixel CMOS) or NIR (256 pixel InGaAs) detector with a time resolution of ~ 250 fs. Chirp and time-zero corrected spectra and multiexponential kinetic fits were acquired and manipulated using SurfaceExplorer software (Ultrafast Systems). Energy dependent spectra were achieved in like fashion, and by adjusting the pump neutral density filter to vary the power from 0.05-0.4 mW, measured near the sample location with a power meter (ThorLabs PM100A).

Photovoltaic devices were constructed using indium tin oxide (ITO)-coated glass slides (Kinetic Co.) which were cleaned by ultrasonic treatment in sodium dodecyl sulfate, deionized water, isopropyl alcohol, and acetone (15 minutes each). Cleaned ITO slides were then placed in an oxygen plasma cleaner (Harrick PDC-32G) for 20 minutes. PEDOT:PSS was spin-coated (5000 rpm, 1 minute) onto the prepared slides and annealed on a hot plate (130 °C, 20 minutes). The

active layer was prepared by dissolving the donor material with the desired ratio of $PC_{71}BM$ in chlorobenzene (18 mg/ml in total) and stirred overnight at 60 °C in an argon-filled MBraun glovebox. The homogeneous solution was spin-coated onto the PEDOT:PSS layer (1000 rpm, 1 minute) in the glovebox and then dried overnight at room temperature under high vacuum. Lithium fluoride (0.5 nm) and aluminum (100 nm) were deposited in sequence using a high vacuum thermal evaporator. The cathode was patterned using a copper mask which restricted the pixel size to 0.07 cm^2.

Current density-voltage (J-V) plots were achieved using a Keithley 2400 source measurement unit (SMU) operating under AM 1.5 illumination with incident power density of 100 mW/cm^2 supplied by a xenon arc lamp power supply (Oriel Instruments). Incident photon to current efficiency (IPCE) measurements were conducted using monochromatic light supplied from a xenon arc lamp passed through a monochromator (Oriel Instruments). Source intensity at 10 nm increments was measured with a power meter (S350, UDT Instruments) and calibrated silicon detector (221, UDT Instruments), while a Keithley 2400 source meter, with no bias applied, was used to measure the current at each wavelength. All photovoltaic characterization measurements were performed in air. Atomic force microscopy was performed using a Veeco Innova microscope in tapping mode with a silicon tip (8 nm radius) at 325 kHz and a force constant of ~ 40 N/m (MikroMasch USA).

All calculations were performed using density function theory (DFT), implemented with Gaussian 09, Rev. C.01. Geometries were optimized using the B3LYP functional with varying basis sets (6-31G(d) for C, H, O, N; 6-31+G(d) for S; SDD for Pt). 2-Ethylhexyloxy and 4-octyloxyphenyl solubilizing groups were replaced with methyl groups to ease computation expense. Time-dependent DFT calculations were performed on similarly optimized structures,

with the same basis set and level of theory. Structures, orbitals and charge difference density plots were imaged and presented using Chemcraft v. 1.8.

RESULTS

UV-Visible Absorption Spectroscopy. Ground-state absorption spectra were obtained in THF solution for both monomer precursors (Pt-Br_2 and BDT-Sn_2), model complex (BDT-Pt_2) and polymer (p-BDT-Pt, $M_n \sim 5000$ g/mol, PDI = 1.5-2), and are presented in Figure 1. The absorption spectrum of Pt-Br_2 is dominated by a broad band between 250-400 nm with a tail extending as far as 500 nm. The broadness of this feature is likely the result of the mixing of several transitions including π–π* and MLCT. The rigid nature of the fused BDT core on the BDT-Sn_2 monomer results in structured absorptions around 300 and 350 nm, due to π–π* transitions. As the two precursors are combined into the model complex BDT-Pt_2, the absorption red-shifts as the conjugation increases. In particular, the π–π* transition from the BDT core red-shifts by 140 nm and assumes the lowest energy transition in the new compound. Transitions imparted from the cyclometalated platinum chromophore are also evident, but their energy shift with conjugation is less dramatic (only about 10-20 nm). An impressive increase in extinction coefficient relative to the two precursors is also observed for the model complex, the result of coupling of the two chromophores with a concomitant increase in the transition dipole. The absorption spectrum of the polymer p-BDT-Pt assumes a similar structure to that of the model complex with both high and low energy maxima red-shifted as conjugation is further extended. The low energy transition, arising from the π–π* transition of the conjugated electronic system, red-shifts about 90 nm from the complementary transition in the model complex. The decrease in the polymer extinction coefficient relative to the model complex is in some respect an artifact as that of the polymer is

calculated per polymer repeat unit (one Pt unit) while that of the model is calculated per molecule (two Pt units).

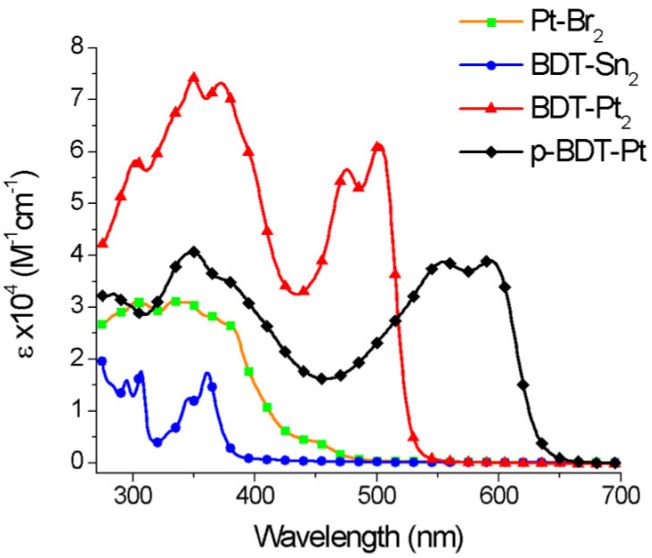

Figure 1. UV-visible absorption spectra of compounds studied: Pt-Br_2 (green squares), BDT-Sn_2 (blue circles), BDT-Pt_2 (red triangles), p-BDT-Pt (black diamonds).

Photoluminescence Spectroscopy. Steady state emission measurements were conducted for all compounds in THF after adjusting the solution absorption to ~ 0.1 optical density. Absorption-emission comparative spectra for these compounds containing a cyclometalated platinum moiety are presented in Figure 2 and relevant photophysical data for all compounds studied is listed in Table 1. As a large motivation for this work focused on the triplet state, it was hoped that evidence of such would be clear from the existence of phosphorescence emission. To probe phosphorescence emission, samples were degassed by bubbling argon for at least 30 minutes to eliminate dissolved oxygen. The large Stokes shift for the emission from monomer Pt-Br_2 is evidence of room temperature phosphorescence, as has been previously observed for similar orthometallated platinum complexes.[25,41-42] The emission also increases in intensity when the solution is degassed, providing further evidence of phosphorescence emission.

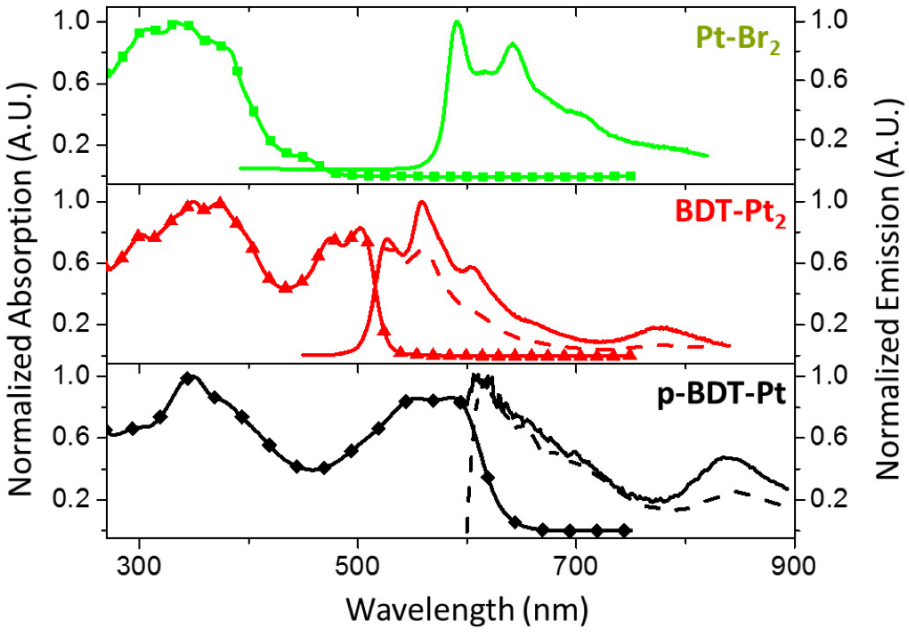

Figure 2. Absorption (solid lines with symbols) and emission (air saturated: dashed lines, degassed: solid lines) spectra of compounds studied at room temperature under argon atmosphere: Pt-Br_2 (green), BDT-Pt_2 (red), p-BDT-Pt (black).

The spectra of the model complex (BDT-Pt_2) and polymer (p-BDT-Pt) under air saturated conditions (Figure 2 dashed lines) show weak emission ($\Phi < 1\%$) with small Stokes shifts and short lifetimes ($\tau < 100$ ps), indicating that this emission is likely fluorescence. As shown by the monomer sample, intersystem crossing (ISC) to the triplet state is expected to be a dominant decay mechanism, and thus weak fluorescence is unsurprising. Upon degassing (Figure 2 solid lines), the presence of a new low energy emission was observed at 780 nm for BDT-Pt_2 and 843 nm for p-BDT-Pt and the emission is ascribed to phosphorescence. The phosphorescence band maxima are used to assign the triplet energies of the materials (1.59 eV for BDT-Pt_2 and 1.47 eV for p-BDT-Pt).

Table 1. Absorption and emission properties.

Compound	λ_{max}^{abs} (nm)	ε ($M^{-1}cm^{-1}$)	λ_{max}^{em} (nm)	E_g (eV)	Φ_F [b] (%)	τ_F (ns)	Φ_{Ph} [c] (%)	Φ_Δ [d] (%)
Pt-Br_2	335	31,200	591	2.60 [a]	--	--	22	37
BDT-Sn_2	361	17,400	401	3.09	56	2.9	--	11
BDT-Pt_2	502	61,300	527	2.35	< 1	< 0.1	< 1	85
p-BDT-Pt	593	39,000	623	1.99	< 1	< 0.1	< 1	33

[a] Bandgap for Pt-Br_2 estimated from absorption onset. [b] Fluorescence quantum yield determined in THF with tetraphenylporphyrin in toluene as standard.[43] [c] Single-point phosphorescence quantum yield determined in THF with tris(2,2'-bipyridyl)ruthenium(II) in DI water as standard.[44] Pt-Br_2 was degassed via 5 freeze-pump-thaw cycles prior to the measurement. [d] Singlet oxygen quantum yield determined in $CDCl_3$ with terthiophene in $CDCl_3$ as standard.[45]

Singlet oxygen sensitization experiments were also performed as a qualitative measure of triplet yield. After bubbling oxygen through the solution, the emission was probed from 1200-1350 nm. As triplet states are generated, they are quenched via Dexter energy transfer to ground state O_2, producing excited singlet oxygen, which then decays via phosphorescence. The relative intensity of the singlet oxygen emission compared to an actinometer (terthiophene) provides the singlet oxygen quantum yield (Φ_Δ, Table 1). As expected, all the materials containing platinum were efficient at sensitizing single oxygen, providing further evidence of efficient ISC in these compounds. It is worthwhile to note that the model complex (BDT-Pt_2) had higher Φ_Δ than the polymer (p-BDT-Pt). Because singlet O_2 sensitization is a diffusion-controlled process, this suggests that there may be an additional rapid triplet decay mechanism in the polymer that is not present in the model complex. This will be discussed later.

Electrochemistry. Electrochemical measurements were performed to ascertain the energy levels of highest occupied and lowest unoccupied molecular orbitals (HOMO and LUMO) of these compounds, to predict the energetics of photoinduced charge transfer to acceptors. As cyclic voltammetry measurements were not sufficiently sensitive, differential pulse voltammetry (DPV)

was used to acquire electrochemical properties of the compounds studied and the voltammograms are contained in Figure S14. For those materials used in solar cells, BDT-Pt_2 and p-BDT-Pt, only irreversible oxidation waves were observed. These oxidation potentials were referenced to a Fc/Fc^+ couple (-4.80 eV relative to vacuum)[46] and used as an estimate of HOMO energies. As no reduction waves could be observed, the LUMO energy was estimated by adding the optical bandgap (fluorescence emission maximum) to the HOMO energy. These values are presented in Table 2. Although these LUMO energies seem to align nicely with that of $PCB_{71}M$ (-3.7 eV), it is important to recall that efficient ISC in these compounds will rapidly populate the triplet state. Given that the triplet state is a weaker reductant than the singlet state by 0.5 - 0.8 eV, it is possible that photoinduced electron transfer from the triplet to $PCB_{71}M$ may not be exothermic. This will be discussed later.

Table 2. Energetics of model complex and polymer studied, derived from electrochemistry and fluorescence spectra.

Compound	E_{ox}[a] (V)	HOMO (eV)	E_g[b] (eV)	LUMO (eV)
BDT-Pt_2	0.51	-5.3	2.35	-3.0
p-BDT-Pt	0.63	-5.4	1.99	-3.4

[a]Oxidation half potentials determined using differential pulse voltammetry with films of compounds dropcast onto a 1 mm^2 platinum working electrode in AcCN using 0.1 M NBu_4PF_6 supporting electrolyte, Ag/Ag^+ reference electrode and platinum wire counter electrode. Scans were conducted at 100 mV/s. Reported potentials are referenced to a Fc/Fc^+ internal standard. [b] Bandgaps determined from fluorescence maxima.

Nanosecond Transient Absorption Spectroscopy. To investigate the triplet states and their dynamics in the platinum-containing materials, nanosecond transient absorption (TA) spectroscopy was employed. All samples were studied in argon deoxygenated THF, and were exited with 355 nm, 5 ns pulses (10 mJ/pulse). Comparison of ground state (top) and transient (bottom) absorption of these molecules and their triplet lifetimes are presented in Figure 3 (Pt-Br_2 left, BDT-Pt_2 center, p-BDT-Pt right). All kinetic data including triplet lifetimes (τ_T) are shown in

Table 3. In the TA spectra, appropriate time delays are employed to clearly show triplet decay. For Pt-Br_2 a clear, intense transient absorption appears at ~ 470 nm and decays with a lifetime of 8.19 μs. In the case of BDT-Pt_2, strong transient absorption appears at ~ 775 nm that decays with a 608 ns lifetime. The transient absorption is notably more intense for BDT-Pt_2 and this is likely attributed mostly to the increased triplet-triplet absorptivity of that compound due to its greater conjugation length, although it may also be evidence of a higher triplet yield. In the case of p-BDT-Pt, only a very weak transient absorption was observed. Although the emission experiments (phosphorescence and singlet oxygen sensitization) confirm that the triplet state is populated in p-BDT-Pt, it is likely that the decay of the triplet is rapid. In addition, as shown below, there is evidence that the triplet population in p-BDT-Pt is limited by triplet-triplet annihilation,[47] and this process could be active given the relatively high pulse energies used in the nanosecond TA experiments. Using another TA instrument modified for single-wavelength detection, a transient absorption decay profile was acquired, and the lifetime measured at 328 ns, shorter than for the other platinum-containing compounds.

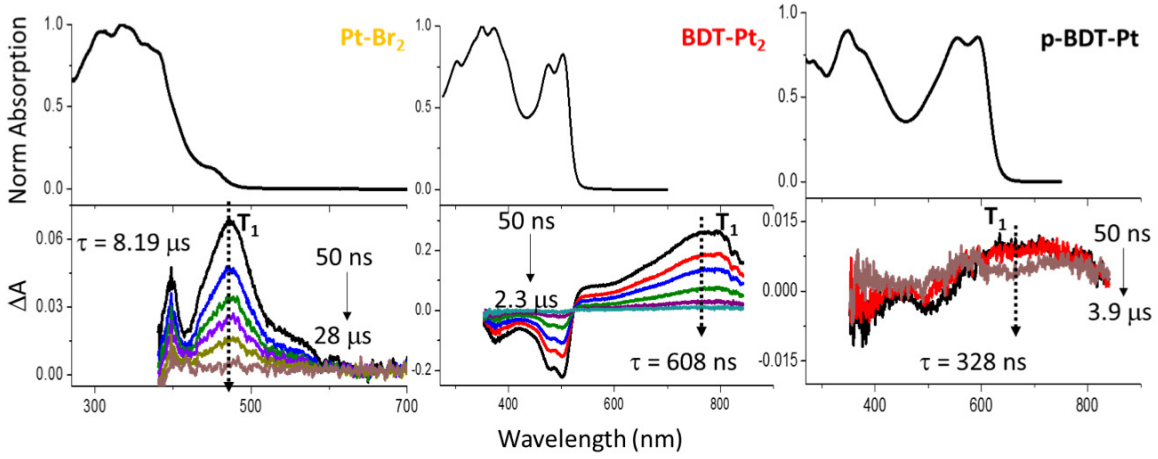

Figure 3. Ground state absorption (top) and nanosecond transient absorption (bottom) of compounds studied: Pt-Br_2 (left), BDT-Pt_2 (center), p-BDT-Pt (right). Transient decays selected

to show optimum decay of triplet state. Ground state and transient absorption spectra collected in THF solution. All samples were excited at 355 nm after deoxygenation with argon.

Picosecond Transient Absorption Spectroscopy. To further probe the excited state dynamics towards to the objective of determining rates of ISC in these compounds, ultrafast TA spectroscopy was employed. Similar to nanosecond experiments, measurements were made in deoxygenated THF and the solution was continuously circulated throughout the measurement. A pump beam of 370 nm and 0.1 μJ pulse energy was used to excite the samples. Comparative ground state (top) and transient (bottom) absorption spectra, along with decay profiles of major transient features are displayed for all platinum-containing compounds in Figure 4, and the relevant kinetic data are collated in Table 3. Curve fitting for all ultrafast TA decay profiles was best achieved using a triexponential decay function with an additional infinite lifetime component (corresponding to the long-lived triplet state). This complex fitting provides important insight into the different processes occurring in these excited states as well as their relative contribution to the overall decay.

Table 3. Kinetic data obtained from transient absorption spectroscopic measurements

Compound	λ (nm)	τ_T [a] (ns)	τ_1 (ps)	A_1 (%)	τ_2 (ps)	A_2 (%)	τ_3 (ps)	A_3 (%)	A_{Inf} (%)	k_{ISC} (s^{-1})
Pt-Br_2	N/A	8190								
	476		0.56	-30	5.83	4	762	9	56	$2.5x10^{12}$
	650		0.22	73	6.85	18	157	2	7	
BDT-Pt_2	N/A	608								
	542		3.13	-15	19.6	-35	1420	8	42	$2.5x10^{11}$
	901		5.03	19	30.5	22	1680	9	51	
p-BDT-Pt	650	328								
	640		1.42	53	19.1	19	633	11	17	> $3x10^{12}$
	909		1.05	39	54.6	25	1610	13	24	

[a] Triplet lifetime obtained via monoexponential decay of data from nanosecond TA instrument (global decay over entire spectral window for Pt-Br_2 and BDT-Pt_2 and single wavelength decay of peak intensity at 650 nm for p-BDT-Pt). Remainder of lifetime and amplitude data obtained via multiexponential decay of data from ultrafast TA instrument. k_{ISC} calculated as $1/\tau_1$ for Pt-Br_2 and BDT-Pt_2.

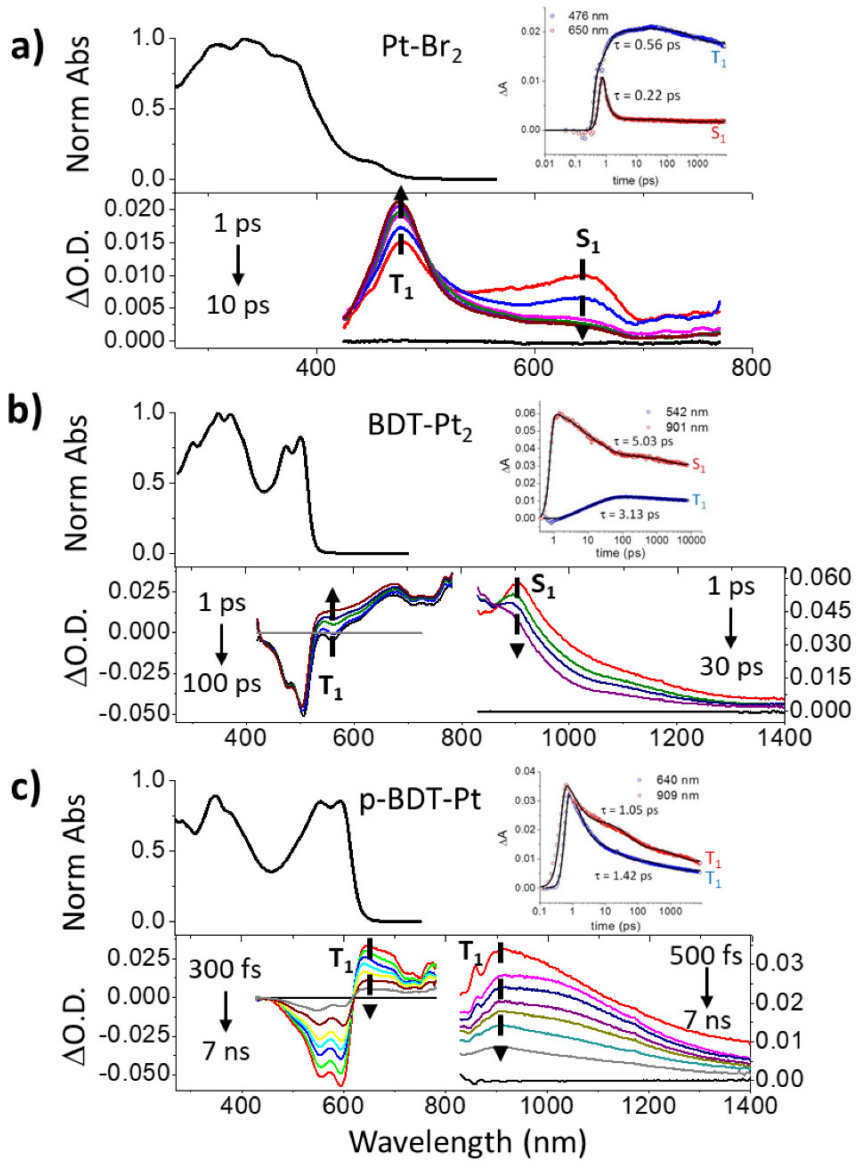

Figure 4. Ground state absorption (top), picosecond transient absorption (bottom), and kinetic profiles (inset) of Pt-Br_2 (a), BDT-Pt_2 (b), and p-BDT-Pt (c). Singlet decay and triplet growth are indicated in TA spectra and kinetic profiles. Ground state and transient absorption spectra collected in THF solution. All samples were excited at 370 nm after deoxygenation.

Figure 4a shows the visible region of the TA profile of Pt-Br_2. From this plot, we identify a short-lived absorption around 650 nm that is fully formed in < 1 ps and decays with a lifetime of ~0.22 ps. Due to its short-lived nature, we assign this peak to the excited singlet state (S_1). Concomitant with this decay (from 1 - 30 ps) is the rise of an absorption ~475 nm. By comparison

with the nanosecond TA (Figure 3), we can confidently assign the 475 nm absorption to the triplet state (T_1). Clearly it can be seen that as S_1 decays T_1 is produced, as is expected when ISC is occurring (see also Figure 4a inset). By analyzing the kinetics at the two wavelengths of interest (Table 3: 476 nm, T_1 growth; 650 nm, S_1 decay), it can be observed that the short lifetime (τ_1) has a dominant influence in the kinetics (compare A_1 vs A_2 and A_3). Note that the most significant lifetime of the decay at 476 nm is the infinite lifetime, as would be expected for T_1 in an experiment at this timescale.

The similarity of the lifetimes at both wavelengths (0.56 ps and 0.22 ps) and the opposite signs of their amplitudes show that these processes occur at nearly the same rate. From previous emission measurements, we suspect that the dominant decay mechanism of S_1 is ISC to T_1. This evidence leads us to assign intersystem crossing as the dominant decay mechanism, with a lifetime of ~ 0.4 ps. This corresponds to a rate constant of ~ 2.5 x 10^{12} s^{-1}, which is very fast for ISC and easily competes with that of fluorescence (typical 10^9 - 10^7 s^{-1})[48] for the dominant decay route.

A similar ground state and transient absorption comparison for the model complex BDT-Pt_2 is shown in Figure 4b. For this analysis it was necessary to expand the detection range to also include the near-IR (800-1400 nm). In the visible region, a clear ground state bleach appears near 500 nm as expected given the strong ground state absorption at the same energy. The rest of the TA spectrum is defined by a broad band that extends into the near-IR and closely correlates with that observed in the nanosecond TA spectrum. In the near-IR portion of the spectrum, a notable absorption appears at around 900 nm, being fully grown after 1 ps. This feature decays with a lifetime of 5 ps and is therefore assigned as S_1. The persistent peak edge that remains after 2 ns is likely part of the broad triplet (T_1) absorption and accounts for the increased A_{Inf} as compared to Pt-Br_2. In the visible region of the spectrum an absorption is observed that grows in with a lifetime

of 3 ps and is in good agreement with the position of T_1 observed in the nanosecond TA. By monitoring the kinetics at 542 nm (T_1 growth) and 901 nm (S_1 decay), we see good agreement in the short lifetime component, τ_1 = 3.13 ps (542 n,) and τ_1 = 5.03 ps (901 nm), see Figure 4b inset and Table 3. Clearly, the decay at 901 nm matches well with the growth at 542 nm, and so we again ascribe this lifetime ($\tau \sim 4$ ps) to intersystem crossing, resulting in a rate constant of ~ 2.5 x 10^{11} s^{-1}. This ISC is also very fast and accounts well for the low fluorescence quantum yield and high singlet oxygen sensitization yield. Interestingly, ISC in BDT-Pt_2 is nearly 100-fold faster than observed for previously studied ortho-metalated conjugated oligomers reported from our lab.[24-25]

The ground state and transient absorption spectra for polymer p-BDT-Pt are shown in Figure 4c. Some similarities exist in this TA spectrum to that of BDT-Pt_2, namely an expected bleach aligning with the energy of ground state absorption (around 600 nm) and a broad absorption stretching from the end of the bleach to past the detection limit of 1400 nm. Unfortunately, in the ultrafast TA spectrum of p-BDT-Pt, no specific features can be identified exclusively as S_1 as represented by fast decay, or T_1 (as fast growth). By contrast, the entire TA bleach and absorption decays with heterogeneous kinetics, with kinetics ranging from a few to several-hundred ps (Table 3) to an end state intensity which is non-zero, indicating the presence of a species with a lifetime > 5 ns. Given this information along with previous evidence of triplet formation (phosphorescence emission, singlet O_2 sensitization), it is possible that for p-BDT-Pt S_1 and T_1 have similar band shapes and are thus indistinguishable. More likely is the possibility that ISC occurs on an ultrafast timescale and the triplet is formed in less than 300 fs ($k_{ISC} > 3x10^{12}$ s^{-1}), and singlet decay is not observed. Through kinetic analysis (Figure 4c inset and Table 3), the peaks at the two wavelengths of analysis (640 and 909 nm) have similar decay profiles and likely represent the same excited

state (T_1). Because ISC is too fast to be observed in p-BDT-Pt, the dominant decay of T_1 ($\tau_1 \sim 1$ ps) is via a mechanism not present in Pt-Br_2 or BDT-Pt_2. As mentioned earlier, triplet-triplet annihilation (TTA) is a common decay mechanism in materials with high triplet concentrations such as organometallic polymers, and thus the fast lifetime observed here may be attributed to this process.

To summarize the results from our ultrafast TA study, S_1 decay was observed in Pt-Br_2 and BDT-Pt_2 at a wavelength unique from the broad triplet absorption, also observed in nanosecond TA measurements. Further, growth of T_1 absorption was also observed on a similar timescale to the decay of S_1, leading to the estimation of k_{ISC}. In the case of p-BDT-Pt, discrete S_1 and T_1 features were not observed and the broad absorption quickly decays to a non-zero value within 7 ns. The lack of observed S_1 decay indicates that ISC is ultrafast in p-BDT-Pt, and the accelerated decay of T_1 observed may be due to TTA. This is further substantiated by the nanosecond TA spectrum of p-BDT-Pt (Figure 3) where the intensity of the first time slice (50 ns) is weak, indicating faster decay of triplets in p-BDT-Pt than in Pt-Br_2 and BDT-Pt_2. The reason that ISC is faster in p-BDT-Pt compared to the model complex BDT-Pt_2 may be that spin-orbit coupling is larger in the polymer due to the higher platinum content in the polymer chains. A similar effect of increased intersystem crossing rate in a platinum-containing polymer compared to model oligomers was previously observed.[49]

Triplet-Triplet Annihilation. As noted above, the triplet absorption of p-BDT-Pt was markedly lower compared to BDT-Pt_2, despite the similarity of the structures. We suspected that the reduced triplet absorption amplitude for the polymer could be due to triplet-triplet annihilation (TTA). Thus, to probe the possibility of TTA in the p-BDT-Pt, transient absorption was used to determine relative triplet population under conditions of variable excitation pulse energy. Figure

5a shows a plot of triplet absorption measured at 650 nm vs. the energy fluence of the pump laser (355 nm) in nanosecond TA. Solutions of BDT-Pt_2 and p-BDT-Pt in THF were degassed and excited with the pump laser at incrementally increasing fluence. For the molecular complex, the triplet absorption increases rapidly with increasing fluence, and then begins to saturate for fluence > 1 mJ/cm^2. By contrast, the triplet absorption of the polymer reaches saturation at less than one third of the intensity of that of the model complex. We postulate that the lower saturation triplet absorption for p-BDT-Pt arises because of exciton annihilation via TTA.

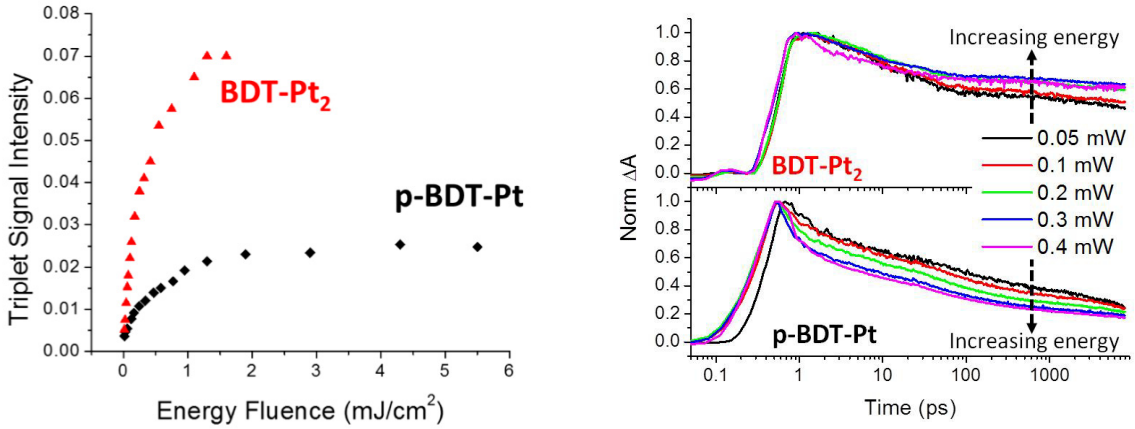

Figure 5. a) Relative triplet absorption as a function of laser fluence for model complex and polymer samples showing an enhanced dependence on excitation energy for polymer samples. Transient signal measured in THF solution using a 5 nanosecond pulsed excitation, λ_{exc} = 355 nm. Samples had matched ground state absorption at the excitation wavelength. b) Transient absorption dynamics comparison with increasing excitation energy (λ_{exc} = 370 nm, 0.05 – 0.4 mW, 1 kHz 120 fs pulses) showing excitation power dependence. Model complex (BDT-Pt_2) monitored at 901 nm and polymer (p-BDT-Pt) monitored at 910 nm in THF solution.

Further evidence for TTA in p-BDT-Pt was obtained by ultrafast TA as shown in Figure 5b and Figure S13. For both BDT-Pt_2 and p-BDT-Pt, the excited state decays were multi-exponential; however, for p-BDT-Pt, there was a distinct ultrafast decay, the amplitude and lifetime of which varied with excitation energy. Figure 5b contains the results of this energy-dependent experiment.

In the case of the polymer (Figure 5b bottom), as the excitation power increases (from 0.05 mW to 0.4 mW), there is a distinct fast decay phase that increases in amplitude significantly, with concomitant loss in amplitude of the long-lifetime component associated with the triplet state. This behavior suggests that there is TTA occurring on an ultrafast timescale, at the expense of the yield of the long-lived triplet state. A similar study on the model complex BDT-Pt_2 reveals some power dependence in the decay; however, the appearance of a distinct fast component that increases in amplitude with energy is not seen.

Photovoltaic Characterization. Bulk heterojunction (BHJ) solar cells composed of varying ratios of donor (BDT-Pt_2 or p-BDT-Pt) and acceptor materials ($PC_{71}BM$) were constructed according to the following architecture: ITO/PEDOT:PSS/active layer/LiF(0.5 nm)/Al(100 nm). The active layer was deposited by spin-casting from a solution of chlorobenzene. Characterization of the photovoltaic performance of the devices was carried out in air within 1 hour of removal from an oxygen-free environment. The solar cells were initially fabricated using BDT-Pt_2 or p-BDT-Pt with $PC_{71}BM$ in a 1:6 ratio (see Figure S15 and Table S2). Interestingly, cells containing the polymer sample p-BDT-Pt, resulted in a higher power conversion efficiency (PCE) (0.70%) than that of model complex BDT-Pt_2 (0.15%). One reason for the lower performance of the BDT-Pt_2 cell may be due to the fact that the active layer based on this material did not form a uniform homogeneous film due to its poor solubility in chlorobenzene.

Having achieved a modest PCE by incorporating p-BDT-Pt in the active layer, BHJ solar cells were fabricated with varying ratios of polymer to $PC_{71}BM$. Representative current density-voltage curves for these devices are displayed in Figure 6a and the relevant measured parameters listed in Table 4. A p-BDT-Pt:$PC_{71}BM$ ratio of 1:9 produced the optimum device with V_{oc} = 0.65 V, J_{sc} = 4.37 mA/cm^2, FF = 36% and PCE = 1.02%. Figure 6b shows the incident photon-to-electron

conversion efficiency (IPCE) for the optimized ratio (1:9) of p-BDT-Pt:$PC_{71}BM$. When compared to the UV-visible absorption spectrum of p-BDT-Pt (Figure 1), it seems likely that the band in the IPCE spectrum corresponds to the polymer absorption. It is worthwhile to note that the modest device efficiency observed is significantly higher than a previous report[24] of donor-acceptor polymers with similar cyclometalated platinum structures, both of which have frontier energy levels with poor alignment to $PC_{71}BM$.

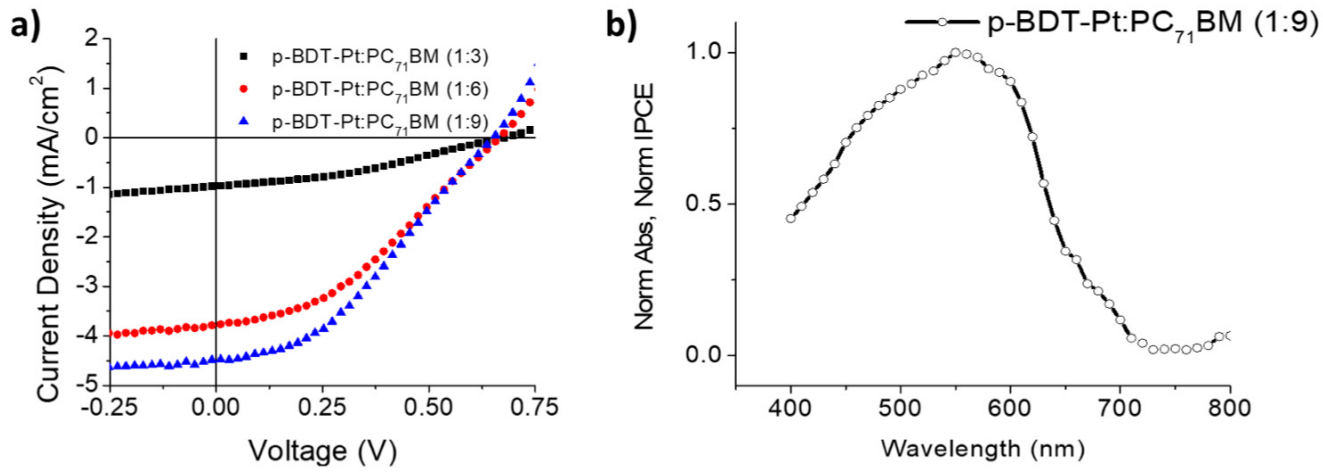

Figure 6. a) Current density-voltage (*J-V*) curves of polymer solar cell devices fabricated with p-BDT-Pt as donor and $PC_{71}BM$ as acceptor in varying ratios. b) Normalized IPCE plot of optimized device with donor-acceptor ratio (1:9).

Table 4. Photovoltaic properties of organic blend photovoltaic cells of model complex and polymer combined with $PC_{71}BM$ at different blend ratios.

Compound	D:A Blend Ratio	V_{oc} (V)	J_{sc} (mA/cm^2)	FF (%)	η (%)
$BDT\text{-}Pt_2$	1:6	0.48	0.90	35	0.15
p-BDT-Pt	1:3	0.67	0.90	35	0.21
	1:6	0.66	3.80	37	0.94
	1:9	0.65	4.37	36	1.02

Device architecture: ITO/PEDOT:PSS/active layer/LiF(0.5 nm)/Al(100 nm). Error ranges: V_{oc} (± 0.02 V), J_{sc} (± 0.02 V), FF (± 2%), η (± 0.03%). Errors are the standard deviation from measurement of 8 pixels for each active material composition.

To further understand the effect of varying donor-acceptor ratio on the device performance, height and phase atomic force microscopy (AFM) images were acquired for the three different p-BDT-Pt:$PC_{71}BM$ ratios of the active layer, and are presented in Figure 7. The height images show a distinct phase separation at the 1:3 ratio, where the $PC_{71}BM$ is in domains that are 200 – 500 nm in size. In the 1:9 ratio, the blend is clearly more homogeneous and the $PC_{71}BM$ appears to be more uniformly distributed within the polymer domains. It was observed that the root-mean-square surface roughness (R_q) decreases as the weight percent of $PC_{71}BM$ increases. Most notably when the ratio decreases from 1:6 to 1:9, the R_q values drop from 2.75 nm to 0.35 nm, indicating a more uniform, homogeneous blend. Phase images demonstrate the same trend as height images. This reduced domain size in the 1:9 ratio active layer no doubt contributes to the enhanced PCE observed in devices constructed with active layers employing that ratio. The trends in the surface morphology of the blends as the amount of $PC_{71}BM$ increases are similar to those observed in a previous studies of platinum containing polymers blended with $PC_{71}BM$.[24,50] The results here strongly suggest that the p-BDT-Pt and $PC_{71}BM$ phases are strongly demixed at lower $PC_{71}BM$ ratios.[51] Only at relatively high $PC_{71}BM$ content does the polymer mix yielding a relatively smooth film morphology.

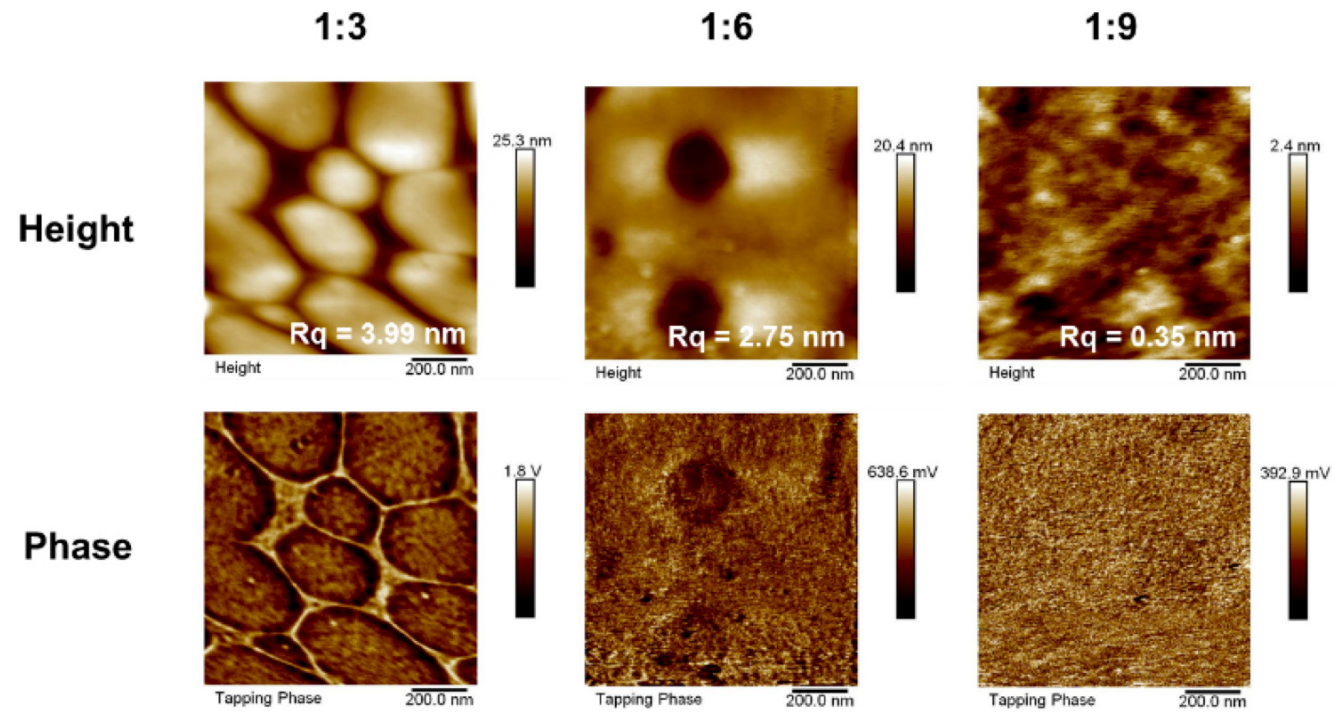

Figure 7. AFM height (top row) and phase (bottom row) images of the active layer of devices with varying donor-acceptor ratios. Root-mean square surface roughness (R_q) values are shown in the lower right of height images.

DISCUSSION

This paper reports an investigation of the photophysical and photovoltaic properties of a conjugated polymer that features BDT units alternating with an ortho-metalated Pt(II) center. The properties of the polymer are compared to those of a structurally defined molecular complex featuring the BDT moiety flanked by two orthometalated Pt(II) units. Both materials exhibit strong visible absorption, due to the extended π-conjugation between the BDT and orthometalated units. Noteworthy is the fact that the p-BDT-Pt exhibits a significantly red-shifted absorption (~90 nm), signaling a further increase in delocalization in the polymer compared to the molecular complex. The model complex BDT-Pt_2 features two well-defined emission bands, one attributed to fluorescence (527 nm, 2.35 eV) and weak, longer wavelength emission (780 nm, 1.58 eV) that can be assigned to phosphorescence. The difference in energy of the emissions signals that the

singlet-triplet (S-T) splitting is ~0.77 eV, which is in accord with other π-conjugated systems.[52] The emission of the polymer p-BDT-Pt is weaker, but it is still possible to discern fluorescence (623 nm, 1.99 eV) and phosphorescence (843 nm, 1.47 eV) bands. The S-T splitting can be estimated as ~0.55 eV, which is less than the model. The lower S-T splitting can also be due to the increased conjugation in the polymer compared to BDT-Pt_2.

The low fluorescence quantum yields and observation of phosphorescence from BDT-Pt_2 and p-BDT-Pt are consistent with efficient singlet to triplet intersystem crossing (ISC). This hypothesis is supported by the fact that both materials exhibit relatively high singlet oxygen quantum yields (Table 1); these values reflect a lower limit on the intersystem crossing efficiency. In the case of p-BDT-Pt the singlet oxygen yield is lower, but this may be due to the fact that the singlet oxygen yield depends on diffusional quenching of the triplet state by ground state oxygen, and due to the comparatively short triplet lifetime of the polymer (~328 ns) the triplet quenching may be inefficient.[53] The transient absorption studies clearly show that ISC is very rapid in BDT-Pt_2, occurring with a rate of ~2.5 x 10^{11} s^{-1}. As noted above, this rate is considerably faster than reported for other conjugated oligomers featuring orthometalated Pt(II) centers.[25] One possible reason for the difference in ISC rate could be the degree of donor-acceptor interaction that is involved in the conjugated system. In a previous study, we reported a correlation between donor-acceptor interaction and the ISC rate in a series of Pt(II) substituted conjugated oligomers.[54] This study showed that when there is a strong donor-acceptor interaction, the ISC rate is slowed. By contrast, in the BDT-Pt_2 oligomer, there is little donor-acceptor interaction and the previous study would point to a fast ISC rate being promoted by the heavy metal centers.[54] Even more surprising is the fact that the ultrafast transient absorption of p-BDT-Pt does not reveal any distinguishable features or dynamics that can be assigned to ISC. The difference spectrum that is observed for p-

BDT-Pt at 200 fs after excitation remains essentially the same out to 7 ns, except for a decay in amplitude. From this we conclude that ISC is extraordinarily fast in the polymer ($k > 3 \times 10^{12}$ s^{-1}) and that the transient absorption is due to the triplet state, which decays via non-radiative channels including triplet-triplet annihilation due to multiple triplet excitons that are produced on a single chain.[47,55]

There has been continuing interest in the relationship of singlet-triplet intersystem crossing, triplet excitons, and the overall performance of organic solar cells.[14,17,56-57] One goal of this study was to explore the BTD substituted, Pt(II) containing polymer in solar cells and to assess what role (if any) the triplet state would play in the cell performance. This study includes some results from prototype solar cells constructed using p-BDT-Pt blended with $PCB_{70}M$ as an electron acceptor. Although the photovoltaic response is low, it is observed that the efficiency increases with increasing acceptor content in the blends. The dependence on acceptor concentration appears to be at least partially due to the length scale of the phase separation in the blends, with nanoscale mixing occurring at higher $PCB_{70}M$ loading.

It is useful to consider the energetics of charge transfer from p-BDT-Pt to $PCB_{70}M$ via the singlet and triplet states of the polymer. Based on the difference in the oxidation potential of p-BDT-Pt and the reduction potential of $PCB_{70}M$,[58] the charge transfer state energy is estimated as ~1.7 eV. This means that charge transfer from the p-BDT-Pt singlet state (1.99 eV) is exothermic, but transfer from the triplet state (1.47 eV) is not thermodynamically favored. Given that photocurrent is observed, we can only conclude that charge transfer must occur in a very fast timescale from the singlet state, prior to intersystem crossing.

SUMMARY AND CONCLUSIONS

In order to further investigate the effect of long lived triplet excitons on the photovoltaic properties of organic blend solar cells, a novel conjugated small molecule (BDT-Pt_2) and polymer (p-BDT-Pt) were synthesized incorporating electron-rich cyclometalated platinum(II) and benzodithiophene chromophores. The presence of the platinum heavy metal allowed ready access to triplet excited states in these compounds as evidenced by their weak fluorescence and room temperature phosphorescence under deoxygenated conditions. Ultrafast transient absorption experiments revealed a very fast intersystem crossing rate on the order of 10^{11}-10^{12} s^{-1} ($\tau \sim 0.5$-5 ps), indicating that most excited states in these systems will be triplet in nature. Estimation placed triplet energies of both small molecule and polymer at or below the energy of the charge transfer state, likely leading to inefficient photoinduced electron transfer in the blends. However, a clear distinction was observed between organic solar cells constructed with BDT-Pt_2 and p-BDT-Pt, the latter achieving a PCE of > 1%, at least 6 times higher than the small molecule, even though the triplet energy of the polymer is lower.

Acknowledgments

We acknowledge the National Science Foundation for support of this work (Grant CHE-1904288).

REFERENCES

1. Morton, O., Solar Energy: A New Day Dawning?: Silicon Valley Sunrise. *Nature* **2006,** *443*, 19-22,
2. National Renewable Energy Laboratory, Best Research Cell Efficiencies. https://www.nrel.gov/pv/cell-efficiency.html.
3. Zhao, W.; Li, S.; Yao, H.; Zhang, S.; Zhang, Y.; Yang, B.; Hou, J., Molecular Optimization Enables over 13% Efficiency in Organic Solar Cells. *J. Am. Chem. Soc.* **2017,** *139*, 7148-7151, 10.1021/jacs.7b02677.

4. Yue, Q.; Liu, W.; Zhu, X., N-Type Molecular Photovoltaic Materials: Design Strategies and Device Applications. *J. Am. Chem. Soc.* **2020,** *142*, 11613-11628, 10.1021/jacs.0c04084.

5. Liu, Q.; Jiang, Y.; Jin, K.; Qin, J.; Xu, J.; Li, W.; Xiong, J.; Liu, J.; Xiao, Z.; Sun, K.; Yang, S.; Zhang, X.; Ding, L., 18% Efficiency Organic Solar Cells. *Science Bulletin* **2020,** *65*, 272-275, https://doi.org/10.1016/j.scib.2020.01.001.

6. Zhan, L.; Li, S.; Lau, T.-K.; Cui, Y.; Lu, X.; Shi, M.; Li, C.-Z.; Li, H.; Hou, J.; Chen, H., Over 17% Efficiency Ternary Organic Solar Cells Enabled by Two Non-Fullerene Acceptors Working in an Alloy-Like Model. *Energ. Env. Sci.* **2020,** *13*, 635-645, 10.1039/C9EE03710A.

7. Cui, Y.; Yao, H.; Hong, L.; Zhang, T.; Tang, Y.; Lin, B.; Xian, K.; Gao, B.; An, C.; Bi, P.; Ma, W.; Hou, J., Organic Photovoltaic Cell with 17% Efficiency and Superior Processability. *National Science Review* **2020,** *7*, 1239-1246, 10.1093/nsr/nwz200.

8. Tang, C. W., Two-Layer Organic Photovoltaic Cell. *App. Phys. Lett.* **1986,** *48*, 183, 10.1063/1.96937.

9. Deibel, C.; Dyakonov, V.; Brabec, C. J., Organic Bulk-Heterojunction Solar Cells. *IEEE Journal of Selected Topics in Quantum Electronics* **2010,** *16*, 1517-1527, 10.1109/JSTQE.2010.2048892.

10. Soci, C.; Hwang, I. W.; Moses, D.; Zhu, Z.; Waller, D.; Gaudiana, R.; Brabec, C. J.; Heeger, A. J., Photoconductivity of a Low-Bandgap Conjugated Polymer. *Adv. Funct. Mater.* **2007,** *17*, 632-636, 10.1002/adfm.200600199.

11. Kang, X.; Zhou, D.; Wang, Q.; Zhu, D.; Bao, X.; Yuan, X.; Liu, F.; Li, Y.; Qiao, S.; Yang, R., Rational Design of Low Band Gap Polymers for Efficient Solar Cells with High Open-Circuit Voltage: The Profound Effect of Me and Cl Substituents with a Similar Van Der Waals Radius. *ACS Appl. Mater. Interfaces* **2019,** *11*, 48155-48161, 10.1021/acsami.9b18278.

12. Brabec, C. J., Plastic Solar Cells. *Adv. Funct. Mater.* **2001,** *11*, 15-26, 10.1002/1616-3028(200102)11:1<15::AID-ADFM15>3.0.CO;2-A.

13. Gouterman, M.; Holten, D., Electron Transfer from Photoexcited Singlet and Triplet Bacteriopheophytin—Ii. Theoretical. *Photochem. Photobiol.* **1977,** *25*, 85-92, 10.1111/j.1751-1097.1977.tb07427.x.

14. Guo, F.; Kim, Y. G.; Reynolds, J. R.; Schanze, K. S., Platinum-Acetylide Polymer Based Solar Cells: Involvement of the Triplet State for Energy Conversion. *Chem. Commun.* **2006**, 1887-9, 10.1039/b516086c.

15. Silverman, E. E.; Cardolaccia, T.; Zhao, X.; Kim, K.-Y.; Haskins-Glusac, K.; Schanze, K. S., The Triplet State in Pt-Acetylide Oligomers, Polymers and Copolymers. *Coord. Chem. Rev.* **2005,** *249*, 1491-1500, 10.1016/j.ccr.2004.11.020.

16. Marco Montalti, A. C., Luca Prodi, M. Teresa Gandolfi, *Handbook of Photochemistry, 3rd Edition*. Taylor and Francis: 2006.

17. Mei, J.; Ogawa, K.; Kim, Y. G.; Heston, N. C.; Arenas, D. J.; Nasrollahi, Z.; McCarley, T. D.; Tanner, D. B.; Reynolds, J. R.; Schanze, K. S., Low-Band-Gap Platinum Acetylide Polymers as Active Materials for Organic Solar Cells. *ACS Appl. Mater. Interfaces* **2009,** *1*, 150-61, 10.1021/am800104k.

18. Wang, Q.; He, Z.; Wild, A.; Wu, H.; Cao, Y.; U, S. S.; Chui, C. H.; Wong, W. Y., Platinum-Acetylide Polymers with Higher Dimensionality for Organic Solar Cells. *Chem. Asian J.* **2011,** *6*, 1766-77, 10.1002/asia.201100111.

19. Goswami, S.; Wicks, G.; Rebane, A.; Schanze, K. S., Photophysics and Non-Linear Absorption of Au(I) and Pt(II) Acetylide Complexes of a Thienyl-Carbazole Chromophore. *Dalton Trans.* **2014,** *43*, 17721-8, 10.1039/c4dt02123a.

20. He, W.; Livshits, M. Y.; Dickie, D. A.; Zhang, Z.; Mejiaortega, L. E.; Rack, J. J.; Wu, Q.; Qin, Y., "Roller-Wheel"-Type Pt-Containing Small Molecules and the Impact of "Rollers" on Material Crystallinity, Electronic Properties, and Solar Cell Performance. *J. Am. Chem. Soc.* **2017,** *139*, 14109-14119, 10.1021/jacs.7b05801.
21. Xu, L.; Ho, C.-L.; Liu, L.; Wong, W.-Y., Molecular/Polymeric Metallaynes and Related Molecules: Solar Cell Materials and Devices. *Coord. Chem. Rev.* **2018,** *373*, 233-257, 10.1016/j.ccr.2017.10.015.
22. Haque, A.; Al-Balushi, R. A.; Al-Busaidi, I. J.; Khan, M. S.; Raithby, P. R., Rise of Conjugated Poly-ynes and Poly(Metalla-ynes): From Design through Synthesis to Structure–Property Relationships and Applications. *Chem. Rev.* **2018,** *118*, 8474-8597, 10.1021/acs.chemrev.8b00022.
23. Clem, T. A.; Kavulak, D. F. J.; Westling, E. J.; Fréchet, J. M. J., Cyclometalated Platinum Polymers: Synthesis, Photophysical Properties, and Photovoltaic Performance. *Chem. Mater.* **2010,** *22*, 1977-1987, 10.1021/cm9029038.
24. Goswami, S.; Gish, M. K.; Wang, J.; Winkel, R. W.; Papanikolas, J. M.; Schanze, K. S., Π-Conjugated Organometallic Isoindigo Oligomer and Polymer Chromophores: Singlet and Triplet Excited State Dynamics and Application in Polymer Solar Cells. *ACS Appl. Mater. Interfaces* **2015,** *7*, 26828-26838, 10.1021/acsami.5b09041.
25. Goswami, S.; Winkel, R. W.; Alarousu, E.; Ghiviriga, I.; Mohammed, O. F.; Schanze, K. S., Photophysics of Organometallic Platinum(II) Derivatives of the Diketopyrrolopyrrole Chromophore. *J Phys Chem A* **2014,** *118*, 11735-43, 10.1021/jp509987p.
26. Liao, C.-Y.; Chen, C.-P.; Chang, C.-C.; Hwang, G.-W.; Chou, H.-H.; Cheng, C.-H., Synthesis of Conjugated Polymers Bearing Indacenodithiophene and Cyclometalated Platinum(II) Units

and Their Application in Organic Photovoltaics. *Solar Energy Materials and Solar Cells* **2013,** *109*, 111-119, 10.1016/j.solmat.2012.09.033.

27. Xu, X.; Feng, K.; Bi, Z.; Ma, W.; Zhang, G.; Peng, Q., Single-Junction Polymer Solar Cells with 16.35% Efficiency Enabled by a Platinum(II) Complexation Strategy. *Adv. Mater.* **2019,** *31*, 1901872, 10.1002/adma.201901872.
28. Yao, H.; Ye, L.; Zhang, H.; Li, S.; Zhang, S.; Hou, J., Molecular Design of Benzodithiophene-Based Organic Photovoltaic Materials. *Chem. Rev.* **2016,** *116*, 7397-7457, 10.1021/acs.chemrev.6b00176.
29. Ouyang, X.; Peng, R.; Ai, L.; Zhang, X.; Ge, Z., Efficient Polymer Solar Cells Employing a Non-Conjugated Small-Molecule Electrolyte. *Nat Photon* **2015,** *9*, 520-524, 10.1038/nphoton.2015.126.
30. Yao, H.; Zhao, W.; Zheng, Z.; Cui, Y.; Zhang, J.; Wei, Z.; Hou, J., PBDT-TSR: A Highly Efficient Conjugated Polymer for Polymer Solar Cells with a Regioregular Structure. *Journal of Materials Chemistry A* **2016,** *4*, 1708-1713, 10.1039/C5TA08614K.
31. Zhao, W.; Qian, D.; Zhang, S.; Li, S.; Inganäs, O.; Gao, F.; Hou, J., Fullerene-Free Polymer Solar Cells with over 11% Efficiency and Excellent Thermal Stability. *Adv. Mater.* **2016,** *28*, 4734-4739, 10.1002/adma.201600281.
32. Chen, W.; Huang, G.; Li, X.; Li, Y.; Wang, H.; Jiang, H.; Zhao, Z.; Yu, D.; Wang, E.; Yang, R., Revealing the Position Effect of an Alkylthio Side Chain in Phenyl-Substituted Benzodithiophene-Based Donor Polymers on the Photovoltaic Performance of Non-Fullerene Organic Solar Cells. *ACS Appl. Mater. Interfaces* **2019,** *11*, 33173-33178, 10.1021/acsami.9b07112.

33. Hualong Pan, Y. L., Yiliang Wu, Ping Liu, Beng S. Ong, Shiping Zhu, Gu Xu, Low-Temperature, Solution-Procesed, High-Mobility Polymer Semiconductors for Thin-Film Transistors. *J. Am. Chem. Soc.* **2007,** *129*, 4112-4113,

34. Li, M.; Ni, W.; Wan, X.; Zhang, Q.; Kan, B.; Chen, Y., Benzo[1,2-B:4,5-B′]Dithiophene (BDT)-Based Small Molecules for Solution Processed Organic Solar Cells. *J. Mater. Chem. A* **2015,** *3*, 4765-4776, 10.1039/c4ta06452f.

35. Liu, Y.; Wan, X.; Wang, F.; Zhou, J.; Long, G.; Tian, J.; Chen, Y., High-Performance Solar Cells Using a Solution-Processed Small Molecule Containing Benzodithiophene Unit. *Adv Mater* **2011,** *23*, 5387-91, 10.1002/adma.201102790.

36. Yongye Liang, Y. W., Danqin Feng, Szu-Ting Tsai, Hae-Jung Son, Gang Li, Luping Yu, Development of New Semiconducting Polymers for High Performance Solar Cells. *J. Am. Chem. Soc.* **2009,** *131*, 56-57,

37. Lee, J.; Kim, J.-H.; Moon, B.; Kim, H. G.; Kim, M.; Shin, J.; Hwang, H.; Cho, K., Two-Dimensionally Extended π-Conjugation of Donor–Acceptor Copolymers Via Oligothienyl Side Chains for Efficient Polymer Solar Cells. *Macromolecules* **2015,** *48*, 1723-1735, 10.1021/acs.macromol.5b00056.

38. Zhang, M.; Gu, Y.; Guo, X.; Liu, F.; Zhang, S.; Huo, L.; Russell, T. P.; Hou, J., Efficient Polymer Solar Cells Based on Benzothiadiazole and Alkylphenyl Substituted Benzodithiophene with a Power Conversion Efficiency over 8%. *Adv Mater* **2013,** *25*, 4944-9, 10.1002/adma.201301494.

39. Zhang, S.; Ye, L.; Hou, J., Breaking the 10% Efficiency Barrier in Organic Photovoltaics: Morphology and Device Optimization of Well-Known PBDTT Polymers. *Adv. Energy Mater.* **2016,** *6*, 1502529-n/a, 10.1002/aenm.201502529.

40. Fu, H.; Wang, Z.; Sun, Y., Polymer Donors for High-Performance Non-Fullerene Organic Solar Cells. *Angewandte Chemie International Edition* **2019,** *58*, 4442-4453, 10.1002/anie.201806291.

41. Murphy, L.; Williams, J. A. G., Luminescent Platinum Compounds: From Molecules to Oleds. In *Molecular Organometallic Materials for Optics*, Bozec, H.; Guerchais, V., Eds. Springer Berlin Heidelberg: Berlin, Heidelberg, 2010; pp 75-111.

42. Kozhevnikov, D. N.; Kozhevnikov, V. N.; Shafikov, M. Z.; Prokhorov, A. M.; Bruce, D. W.; Gareth Williams, J. A., Phosphorescence Vs Fluorescence in Cyclometalated Platinum(Ii) and Iridium(Iii) Complexes of (Oligo)Thienylpyridines. *Inorg. Chem.* **2011,** *50*, 3804-3815, 10.1021/ic200210e.

43. Seybold, P. G.; Gouterman, M., Porphyrins: XIII: Fluorescence Spectra and Quantum Yields. *J. Mol. Spect.* **1969,** *31*, 1-13, 10.1016/0022-2852(69)90335-X.

44. Suzuki, K.; Kobayashi, A.; Kaneko, S.; Takehira, K.; Yoshihara, T.; Ishida, H.; Shiina, Y.; Oishi, S.; Tobita, S., Reevaluation of Absolute Luminescence Quantum Yields of Standard Solutions Using a Spectrometer with an Integrating Sphere and a Back-Thinned CCD Detector. *Phys. Chem. Chem. Phys.* **2009,** *11*, 9850-60, 10.1039/b912178a.

45. Wilkinson, F.; Helman, W. P.; Ross, A. B., Quantum Yields for the Photosensitized Formation of the Lowest Electronically Excited Singlet State of Molecular Oxygen in Solution. *J. Phys. Chem. Ref. Data* **1993,** *22*, 113, 10.1063/1.555934.

46. Cardona, C. M.; Li, W.; Kaifer, A. E.; Stockdale, D.; Bazan, G. C., Electrochemical Considerations for Determining Absolute Frontier Orbital Energy Levels of Conjugated Polymers for Solar Cell Applications. *Adv. Mater.* **2011,** *23*, 2367-2371, 10.1002/adma.201004554.

47. Goswami, S.; Cekli, S.; Alarousu, E.; Winkel, R. W.; Younus, M.; Mohammed, O. F.; Schanze, K. S., Light-Harvesting Two-Photon-Absorbing Polymers. *Macromolecules* **2020,** *53*, 6279-6287, 10.1021/acs.macromol.0c01035.

48. Lakowicz, J. R., *Principles of Fluorescence Spectroscopy*. Springer: 2006.

49. Cekli, S.; Winkel, R. W.; Schanze, K. S., Effect of Oligomer Length on Photophysical Properties of Platinum Acetylide Donor–Acceptor–Donor Oligomers. *J. Phys. Chem. A* **2016,** *120*, 5512-5521, 10.1021/acs.jpca.6b03977.

50. Goswami, S.; Hernandez, J. L.; Gish, M. K.; Wang, J.; Kim, B.; Laudari, A. P.; Guha, S.; Papanikolas, J. M.; Reynolds, J. R.; Schanze, K. S., Cyclometalated Platinum-Containing Diketopyrrolopyrrole Complexes and Polymers: Photophysics and Photovoltaic Applications. *Chem. Mater.* **2017,** *29*, 8449-8461, 10.1021/acs.chemmater.7b03018.

51. Wang, W. J.; Song, L.; Ren, X. H.; Fan, H. Q.; Moulin, J. F.; Muller-Buschbaum, P., Influence of Solvent Additive 1,8-Octanedithiol on P3ht:Pcbm Solar Cells. *KnE Materials Science* **2018,** *4*, 56-65, 10.18502/kms.v4i2.3038.

52. Köhler, A.; Beljonne, D., The Singlet–Triplet Exchange Energy in Conjugated Polymers. *Adv. Funct. Mater.* **2004,** *14*, 11-18, 10.1002/adfm.200305032.

53. Gundogan, A. S.; Jagadesan, P.; Schanze, K. S., Photophysics of Oligothiophenes End-Capped with Platinum(II) Auxochromes. *ChemPhotoChem* **2021,** *5*, 160-166, 10.1002/cptc.202000123.

54. Cekli, S.; Winkel, R. W.; Alarousu, E.; Mohammed, O. F.; Schanze, K. S., Triplet Excited State Properties in Variable Gap Pi-Conjugated Donor-Acceptor-Donor Chromophores. *Chem. Sci.* **2016,** *7*, 3621-3631, 10.1039/c5sc04578a.

55. Datko, B. D.; Grey, J. K., Population Dynamics of Multiple Triplet Excitons Revealed from Time-Dependent Fluorescence Quenching of Single Conjugated Polymer Chains. *Scientific Reports* **2019,** *9*, 817, 10.1038/s41598-018-37477-8.

56. Jin, Y.; Zhang, Y.; Liu, Y.; Xue, J.; Li, W.; Qiao, J.; Zhang, F., Limitations and Perspectives on Triplet-Material-Based Organic Photovoltaic Devices. *Adv. Mater.* **2019,** *31*, 1900690, 10.1002/adma.201900690.

57. Luppi, B. T.; Majak, D.; Gupta, M.; Rivard, E.; Shankar, K., Triplet Excitons: Improving Exciton Diffusion Length for Enhanced Organic Photovoltaics. *J. Mater. Chem. A* **2019,** *7*, 2445-2463, 10.1039/C8TA10037C.

58. Kooistra, F. B.; Mihailetchi, V. D.; Popescu, L. M.; Kronholm, D.; Blom, P. W. M.; Hummelen, J. C., New C84 Derivative and Its Application in a Bulk Heterojunction Solar Cell. *Chem. Mater.* **2006,** *18*, 3068-3073, 10.1021/cm052783z.